Dynamic response of large finite and non-symmetrical twodimensional periodic structures

D Duhamel

Dynamic response of large finite and non-symmetrical two-dimensional periodic structures

D. Duhamel
Ecole des Ponts ParisTech, Laboratoire Navier, ENPC/UGE/CNRS,
6 et 8 Avenue Blaise Pascal, Cité Descartes, Champs-sur-Marne, 77455 Marne La Vallée Cedex 2, France
e-mail: **denis.duhamel@enpc.fr**

Abstract

The study of two-dimensional periodic media (periodic along two directions), generally focuses on dispersion curves. For structures of reasonable sizes, for example with a few hundred substructures, it is also possible to calculate their response to external excitations by classical or improved finite element using model reductions such as the Craig-Bampton method. In this work, we determine their response for a large number of substructures. We base ourselves on the Wave Finite Element (WFE) method and extend it to the 2D case, by determining, on a single substructure, the propagation constants and wave modes along a direction for given propagation constants in the transverse direction. When the structure is symmetrical, a very efficient method has been developed using FFT calculations. Here, we extend it to the case of non-symmetrical structures, that is to say whose geometry and composition of a substructure can be arbitrary. Different examples are given for symmetrical and non-symmetrical structures with a large number of substructures.

1 Introduction

Periodic media are often found in industry due to their ease of production and their mechanical properties such as the existence of band gaps for wave propagation. For one-dimensional periodic media, the Wave Finite Element (WFE) such as described in [1–7] allows calculating dispersion curves and the response to external excitations. For two-dimensional periodic structures, early works such as those of [8–11], used the wave finite element method to compute dispersion relations, and to improve their computation, reduced models such as those obtained by the Craig-Bampton method were used by [12–16].

Other authors were interested in obtaining the response of such structures to an external excitation. The cases of infinite domains were considered by [17–22] using various methods such as contour integrals and the method of steepest descent. The case of finite two-dimensional periodic structures is more difficult but in [23–27] there were computed by finite element methods, sometimes with the help of a Craig-Bampton reduction and interpolation strategies to reduce the computational cost, typically for structures with a few hundreds substructures. Other improvements of the usual finite element method such as the partition of unity finite element method described in [28–30], with interpolation functions closer to analytical solutions, could be used for improving the computation. These methods remain limited in the size of the problems which can be solved, for example because of conditioning problems.

In this paper, we consider the calculation of a finite two-dimensional periodic medium made up of a large number of substructures under external excitations. We focus here on the case of substructures without symmetry while the easier case of symmetrical substructures was studied in [31]. The method proposed in this paper will be based on the WFE. By imposing the wavenumber in one direction, we can numerically calculate the wavenumbers and mode shapes associated with propagation in the perpendicular direction. We can thus build a set of waves propagating respectively along the two directions parallel to the sides of the rectangle which will serve as the basis on which we will decompose the solution. Equations are then set for symmetrical and antisymmetrical parts of the boundary condition. Then, an iterative method using the GMRES algorithm combined with the symmetrical solution used as a preconditioner allows to get the

solution for general structures without symmetry. We thus obtain the global solution for a two-dimensional periodic medium with a large number of substructures.

The paper is organised as follows. In section 2, two-dimensional wave modes for periodic media are computed. In section 3, the global wave decomposition is described and used to solve the problem. Numerical examples are given in section 4 before the conclusion in section 5.

2 Two-dimensional wave modes

2.1 Relations on boundary variables

The discrete dynamic equation of a substructure (an elementary period) obtained from a finite element (FE) model at a circular frequency ω and for the time dependence $e^{i\omega t}$ is given by:

$$((1+\xi i)\mathbf{K} - \omega^2\mathbf{M})\mathbf{q} = \mathbf{f} \tag{1}$$

where $\mathbf{K}$ and $\mathbf{M}$ are the stiffness and mass matrices, respectively, ξ is the damping coefficient, $\mathbf{f}$ is the loading vector and $\mathbf{q}$ the vector of the degrees of freedom (DoFs). Introducing the dynamic stiffness matrix $\mathbf{D} = (1+\xi i)\mathbf{K} - \omega^2\mathbf{M}$, decomposing the DoFs into boundary (b) and interior (i) DoFs, and assuming that there are no external forces on the interior nodes, result in the following equation:

$$\begin{bmatrix} \mathbf{D}_{bb} & \mathbf{D}_{bi} \\ \mathbf{D}_{ib} & \mathbf{D}_{ii} \end{bmatrix} \begin{bmatrix} \mathbf{q}_b \\ \mathbf{q}_i \end{bmatrix} = \begin{bmatrix} \mathbf{f}_b \\ \mathbf{0} \end{bmatrix} \tag{2}$$

The interior DoFs can be eliminated using the second row of equation (2), which results in

$$\mathbf{f}_b = \left(\mathbf{D}_{bb} - \mathbf{D}_{bi}\mathbf{D}_{ii}^{-1}\mathbf{D}_{ib}\right)\mathbf{q}_b = \mathbf{D}_b\mathbf{q}_b \tag{3}$$

where only boundary DoFs are considered in the following. The sizes of vectors $\mathbf{q}_q$ and $\mathbf{f}_b$ equals $n_b \times 1$ and $\mathbf{D}_b$ is a matrix of size $n_b \times n_b$ with n_b the number of DoFs on the boundary of a substructure. We drop the b subscript in the following so that for instance $\mathbf{q}_b$ is denoted as $\mathbf{q}$.

The periodic cell is assumed to be meshed with an equal number of nodes on their opposite sides. The boundary DoFs are decomposed into left (L), right (R), bottom (B), top (T) DoFs and associated corners (LB), (RB), (LT) and (RT) as shown in Figure 1. The global vector of boundary DoFs of size $n_b \times 1$ is decomposed as

$${}^T\mathbf{q} = \left({}^T\mathbf{q}_{LB} \quad {}^T\mathbf{q}_L \quad {}^T\mathbf{q}_{LT} \quad {}^T\mathbf{q}_{RB} \quad {}^T\mathbf{q}_R \quad {}^T\mathbf{q}_{RT} \quad {}^T\mathbf{q}_B \quad {}^T\mathbf{q}_T\right) \tag{4}$$

Note that $n_b = 4n_{LB} + 2n_L + 2n_B$ with n_{LB} the number of DoFs at a corner (the same for the four corners), n_L the number of DoFs at the left boundary without its corners DoFs and n_B the number of DoFs at the bottom boundary without its corners DoFs. The proposed approach consists first of eliminating the DoFs of the lower and upper sides then of expressing all remaining DoFs from a reduced number of DoFs for which an eigenvalue problem will be posed. First, the longitudinal DoFs vector is defined as ${}^t\mathbf{q}_l = \left[{}^t\mathbf{q}_{LB} \quad {}^t\mathbf{q}_L \quad {}^t\mathbf{q}_{LT} \quad {}^t\mathbf{q}_{RB} \quad {}^t\mathbf{q}_R \quad {}^t\mathbf{q}_{RT}\right]$. Thus, equation (3) is rewritten as

$$\begin{bmatrix} \mathbf{D}_{ll} & \mathbf{D}_{lB} & \mathbf{D}_{lT} \\ \mathbf{D}_{Bl} & \mathbf{D}_{BB} & \mathbf{D}_{BT} \\ \mathbf{D}_{Tl} & \mathbf{D}_{TB} & \mathbf{D}_{TT} \end{bmatrix} \begin{bmatrix} \mathbf{q}_l \\ \mathbf{q}_B \\ \mathbf{q}_T \end{bmatrix} = \begin{bmatrix} \mathbf{f}_l \\ \mathbf{f}_B \\ \mathbf{f}_T \end{bmatrix} \tag{5}$$

We are looking for solutions such that the DoFs at the bottom and top boundaries are connected by a propagation constant λ_y along y and using the effort equilibrium at the bottom side of the cell, relations between the transverse DoFs are given by

$$\begin{aligned} \mathbf{q}_T &= \lambda_y \mathbf{q}_B \\ \mathbf{f}_B + \tfrac{1}{\lambda_y}\mathbf{f}_T &= 0 \end{aligned} \tag{6}$$

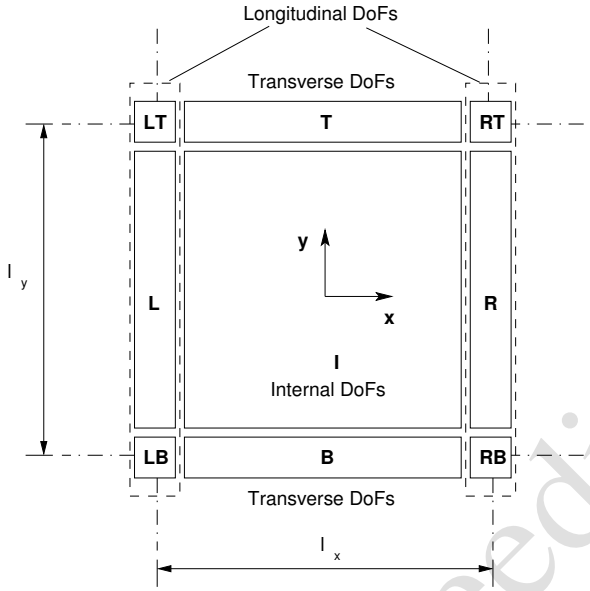

Figure 1: A substructure in the periodic medium

Using (6) and the second and third row of the matrix of equation (5), the first row of equation (5) leads to

$$\begin{aligned} \mathbf{f}_l &= \left[\mathbf{D}_{ll} - (\mathbf{D}_{lB} + \lambda_y \mathbf{D}_{lT}) \left(\mathbf{D}_{BB} + \mathbf{D}_{TT} + \frac{1}{\lambda_y}\mathbf{D}_{TB} + \lambda_y \mathbf{D}_{BT}\right)^{-1} \left(\mathbf{D}_{Bl} + \frac{1}{\lambda_y}\mathbf{D}_{Tl}\right)\right] \mathbf{q}_l \\ &= \mathbf{D}_l \mathbf{q}_l \end{aligned} \tag{7}$$

The sizes of vectors $\mathbf{q}_l$ and $\mathbf{f}_l$ equals $n_l^y \times 1$ and $\mathbf{D}_l$ is a matrix of size $n_l^y \times n_l^y$ with $n_l^y = 4n_{LB} + 2n_L$.

2.2 One-dimensional eigenvalue problem

Introducing the propagation constants λ_x along x and λ_y along y lead to the following relations between longitudinal DoFs

$$\begin{aligned} \mathbf{q}_R &= \lambda_x \mathbf{q}_L \\ \mathbf{q}_{RB} &= \lambda_x \mathbf{q}_{LB} \\ \mathbf{q}_{RT} &= \lambda_x \lambda_y \mathbf{q}_{LB} \\ \mathbf{q}_{LT} &= \lambda_y \mathbf{q}_{LB} \end{aligned} \tag{8}$$

From these conditions (8), it can be seen that all components of the vector $\mathbf{q}_l$ depend on the reduced set of DoFs defined by $\mathbf{q}_r = {}^t\left[{}^t\mathbf{q}_{LB} \quad {}^t\mathbf{q}_L\right]$. This can be expressed as

$$\mathbf{q}_l = \left(\mathbf{W}_0(\lambda_y) + \lambda_x \mathbf{W}_1(\lambda_y)\right) \mathbf{q}_r \tag{9}$$

where the matrices $\mathbf{W}_0(\lambda_y)$ and $\mathbf{W}_1(\lambda_y)$ depend on the propagation constant λ_y and are given by

$$\mathbf{W}_0(\lambda_y) = \begin{bmatrix} \mathbf{I}_{n_{LB}\times n_{LB}} & \mathbf{o}_{n_{LB}\times n_L} \\ \mathbf{o}_{n_L\times n_{LB}} & \mathbf{I}_{n_L\times n_L} \\ \lambda_y \mathbf{I}_{n_{LB}\times n_{LB}} & \mathbf{o}_{n_{LB}L\times n_L} \\ \mathbf{o}_{n_{LB}\times n_{LB}} & \mathbf{o}_{n_{LB}\times n_L} \\ \mathbf{o}_{n_L\times n_{LB}} & \mathbf{o}_{n_L\times n_L} \\ \mathbf{o}_{n_{LB}\times n_{LB}} & \mathbf{o}_{n_{LB}\times n_L} \end{bmatrix} \qquad \mathbf{W}_1(\lambda_y) = \begin{bmatrix} \mathbf{o}_{n_{LB}\times n_{LB}} & \mathbf{o}_{n_{LB}\times n_L} \\ \mathbf{o}_{n_L\times n_{LB}} & \mathbf{o}_{n_L\times n_L} \\ \mathbf{o}_{n_{LB}\times n_{LB}} & \mathbf{o}_{n_{LB}\times n_L} \\ \mathbf{I}_{n_{LB}\times n_{LB}} & \mathbf{o}_{n_{LB}\times n_L} \\ \mathbf{o}_{n_L\times n_{LB}} & \mathbf{I}_{n_L\times n_L} \\ \lambda_y \mathbf{I}_{n_{LB}\times n_{LB}} & \mathbf{o}_{n_{LB}\times n_L} \end{bmatrix} \tag{10}$$

with $\mathbf{I}$ the identity matrix and $\mathbf{o}$ the null matrix. The equilibrium conditions between adjacent cells can be

written as

$$\left(\lambda_x {}^t\mathbf{W}_0(\frac{1}{\lambda_y}) + {}^t\mathbf{W}_1(\frac{1}{\lambda_y})\right)\mathbf{f}_l = 0 \tag{11}$$

Combining (7), (9) and (11), lead to

$$\left(\lambda_x {}^t\mathbf{W}_0(\frac{1}{\lambda_y}) + {}^t\mathbf{W}_1(\frac{1}{\lambda_y})\right)\mathbf{D}_l(\lambda_y)\left(\mathbf{W}_0(\lambda_y) + \lambda_x\mathbf{W}_1(\lambda_y)\right)\mathbf{q}_r = 0 \tag{12}$$

that can be written as

$$\left(\mathbf{A}_{RL} + \lambda_x(\mathbf{A}_{LL} + \mathbf{A}_{RR}) + \lambda_x^2\mathbf{A}_{LR}\right)\mathbf{q}_r = 0 \tag{13}$$

where

$$\begin{aligned}
\mathbf{A}_{RL}(\lambda_y) &= {}^t\mathbf{W}_1(\tfrac{1}{\lambda_y})\mathbf{D}_l(\lambda_y)\mathbf{W}_0(\lambda_y), \quad \mathbf{A}_{LL}(\lambda_y) &= {}^t\mathbf{W}_0(\frac{1}{\lambda_y})\mathbf{D}_l(\lambda_y)\mathbf{W}_0(\lambda_y)\\
\mathbf{A}_{RR}(\lambda_y) &= {}^t\mathbf{W}_1(\tfrac{1}{\lambda_y})\mathbf{D}_l(\lambda_y)\mathbf{W}_1(\lambda_y), \quad \mathbf{A}_{LR}(\lambda_y) &= {}^t\mathbf{W}_0(\frac{1}{\lambda_y})\mathbf{D}_l(\lambda_y)\mathbf{W}_1(\lambda_y)
\end{aligned} \tag{14}$$

As we have taken a small damping, we always have $|\lambda_x| \neq 1$ and the right-going solutions must have propagation constants λ_x^+ of decreasing amplitude as we move on the right, meaning that

$$|\lambda_x^+| < 1, \tag{15}$$

The left going waves are such that

$$|\lambda_x^-| > 1 \tag{16}$$

This allows to define the eigensolutions

$$\begin{aligned}
\mathbf{\Lambda}^+(\lambda_y) &= [\lambda^+_{\mathtt{x}1}(\lambda_y)\cdots\lambda^+_{\mathtt{x}J_n^+}(\lambda_y)] \quad , \quad \mathbf{\Lambda}^-(\lambda_y) &= [\lambda^-_{\mathtt{x}1}(\lambda_y)\cdots\lambda^-_{\mathtt{x}J_n^-}(\lambda_y)]\\
\mathbf{\Phi}^+_{\mathtt{q}}(\lambda_y) &= [\boldsymbol{\phi}^+_{\mathtt{q}1}(\lambda_y)\cdots\boldsymbol{\phi}^+_{\mathtt{q}J_n^+}(\lambda_y)] \quad , \quad \mathbf{\Phi}^-_{\mathtt{q}}(\lambda_y) &= [\boldsymbol{\phi}^-_{\mathtt{q}1}(\lambda_y)\cdots\boldsymbol{\phi}^-_{\mathtt{q}J_n^-}(\lambda_y)]\\
\mathbf{\Phi}^+_{\mathtt{F}}(\lambda_y) &= [\boldsymbol{\phi}^+_{\mathtt{F}1}(\lambda_y)\cdots\boldsymbol{\phi}^+_{\mathtt{F}J_n^+}(\lambda_y)] \quad , \quad \mathbf{\Phi}^-_{\mathtt{F}}(\lambda_y) &= [\boldsymbol{\phi}^-_{\mathtt{F}1}(\lambda_y)\cdots\boldsymbol{\phi}^-_{\mathtt{F}J_n^-}(\lambda_y)].
\end{aligned} \tag{17}$$

in which $\boldsymbol{\phi}_{\mathtt{qj}}$ is the solution of the eigenproblem (13) and $\boldsymbol{\phi}_{\mathtt{Fj}} = {}^t\begin{bmatrix} {}^t\mathbf{f}_{LB}^j & {}^t\mathbf{f}_L^j \end{bmatrix}$ the associated force vector. Note that J_n^+ is the number of right-going waves and J_n^- is the number of left-going waves such that $J_n^+ + J_n^- = 2n_r^y = 2(n_{LB} + n_L)$ which equals two times the size of the eigenproblem (13).

3 Global wave decomposition and solution

3.1 General decomposition

The solution is searched under the form of waves associated to propagation constants $\lambda_{y,n} = e^{i\pi n/N_y}$ along y, for $-N_y \leq n \leq N_y - 1$, leading to the propagation constants λ_{nj}^{x+} and λ_{nj}^{x-} along x. One notes that $\lambda_{y,-N_y} = e^{-i\pi N_y/N_y} = e^{i\pi N_y/N_y} = \lambda_{y,N_y} = -1$, so that n ends at $N_y - 1$ otherwise the same eigenvalue would be counted twice. Along x one has propagation constants $\lambda_{x,m} = e^{i\pi m/N_x}$, for $-N_x \leq m \leq N_x - 1$, leading to the propagation constants λ_{ml}^{y+} and λ_{ml}^{y-} along y. The force on the boundary X of the substructure

at position (p, q) (with $0 \leq p \leq N_x - 1$ and $0 \leq q \leq N_y - 1$) such as in Figure 2 can then be decomposed as

$$\begin{aligned}\mathbf{f}_X(p,q) &= \sum_{n=-N_y}^{n=N_y-1} e^{i\pi qn/N_y}\left(\mathbf{F}_{Xn}^{x+}(\mathbf{\Lambda}_n^{x+})^p\mathbf{a}_n^{x+} + \mathbf{F}_{Xn}^{x-}(\mathbf{\Lambda}_n^{x-})^{p-(N_x-1)}\mathbf{a}_n^{x-}\right) \\ &+ \sum_{m=-N_x}^{m=N_x-1} e^{i\pi pm/N_x}\left(\mathbf{F}_{Xm}^{y+}(\mathbf{\Lambda}_m^{y+})^q\mathbf{a}_m^{y+} + \mathbf{F}_{Xm}^{y-}(\mathbf{\Lambda}_m^{y-})^{q-(N_y-1)}\mathbf{a}_m^{y-}\right) \end{aligned} \tag{18}$$

where $|\lambda_{nj}^{x+}|, |\lambda_{ml}^{y+}| < 1$, $|\lambda_{nj}^{x-}|, |\lambda_{ml}^{y-}| > 1$. J_n^+, J_n^-, L_m^+, L_m^-, are the number of eigenvalues of their respective eigenproblems. One also has

$$\begin{aligned}\mathbf{\Lambda}_n^{x+} &= diag\left(\lambda_{nj}^{x+}\right)_{j=1\ldots J_n^+}, & \mathbf{\Lambda}_m^{y+} &= diag\left(\lambda_{ml}^{y+}\right)_{l=1\ldots L_m^+}, \\ \mathbf{F}_{Xn}^{x+} &= \left[\mathbf{f}_{Xn1}^{x+}, ..., \mathbf{f}_{Xnj}^{x+}, ..., \mathbf{f}_{XnJ_n^+}^{x+}\right], & \mathbf{F}_{Xm}^{y+} &= \left[\mathbf{f}_{Xm1}^{y+}, ..., \mathbf{f}_{Xml}^{y+} ..., \mathbf{f}_{XmL_m^+}^{y+}\right], \\ \mathbf{a}_n^{x+} &= \left[a_{n1}^{x+}, ..., a_{nj}^{x+}, ..., a_{nJ_n^+}^{x+}\right]^T, & \mathbf{a}_m^{y+} &= \left[a_{m1}^{y+}, ..., a_{ml}^{y+}, ..., a_{mL_m^+}^{y+}\right]^T \end{aligned} \tag{19}$$

Similar expressions can be written for negative-going waves. $\mathbf{a}_n^{x+}, \mathbf{a}_n^{x-}, \mathbf{a}_m^{y+}, \mathbf{a}_m^{y-}$ are the amplitudes of the waves. We avoid taking positive powers of propagation constants of modulus greater than one by modifying the terms associated to left going waves. Now we apply this to the different parts of the global boundary. For instance, the force on the global left boundary can then be decomposed as (since $p = 0$ and $X = L$)

$$\begin{aligned}\mathbf{f}_L(q) &= \sum_{n=-N_y}^{n=N_y-1} e^{i\pi qn/N_y}\left(\mathbf{F}_{Ln}^{x+}\mathbf{a}_n^{x+} - \mathbf{F}_{Rn}^{x-}(\mathbf{\Lambda}_n^{x-})^{-N_x}\mathbf{a}_n^{x-}\right) \\ &+ \sum_{m=-N_x}^{m=N_x-1}\left(\mathbf{F}_{Lm}^{y+}(\mathbf{\Lambda}_m^{y+})^q\mathbf{a}_m^{y+} + \mathbf{F}_{Lm}^{y-}(\mathbf{\Lambda}_m^{y-})^{q-(N_y-1)}\mathbf{a}_m^{y-}\right) \end{aligned} \tag{20}$$

and the force on the right boundary is given by

$$\begin{aligned}\mathbf{f}_R(q) &= \sum_{n=-N_y}^{n=N_y-1} e^{i\pi qn/N_y}\left(-\mathbf{F}_{Ln}^{x+}(\mathbf{\Lambda}_n^{x+})^{N_x}\mathbf{a}_n^{x+} + \mathbf{F}_{Rn}^{x-}\mathbf{a}_n^{x-}\right) \\ &- \sum_{m=-N_x}^{m=N_x-1}(-1)^m\left(\mathbf{F}_{Lm}^{y+}(\mathbf{\Lambda}_m^{y+})^q\mathbf{a}_m^{y+} + \mathbf{F}_{Lm}^{y-}(\mathbf{\Lambda}_m^{y-})^{q-(N_y-1)}\mathbf{a}_m^{y-}\right) \end{aligned} \tag{21}$$

Similar expressions can be written for the bottom and top boundaries.

3.2 Decomposition into symmetrical and antisymmetrical functions

Consider, for example, the force on the left boundary given by (20). The expansion in the first sum contains $2N_y$ set of waves in positive and negative directions, thus a total of $4N_y$ sets of waves. To find the amplitudes, one has the values of the force on N_y substructures on the left and right boundaries, thus only $2N_y$ sets of relations. One must also pay attention to the convergence of the Fourier series. The series converge to the value of the function at a point only if the function is continuous at this point. To take into account all this, the precedent relation is split into its symmetrical and antisymmetrical parts, leading to

$$\mathbf{f}_L(q) = \mathbf{f}_L^s(q) + \mathbf{f}_L^a(q) \tag{22}$$

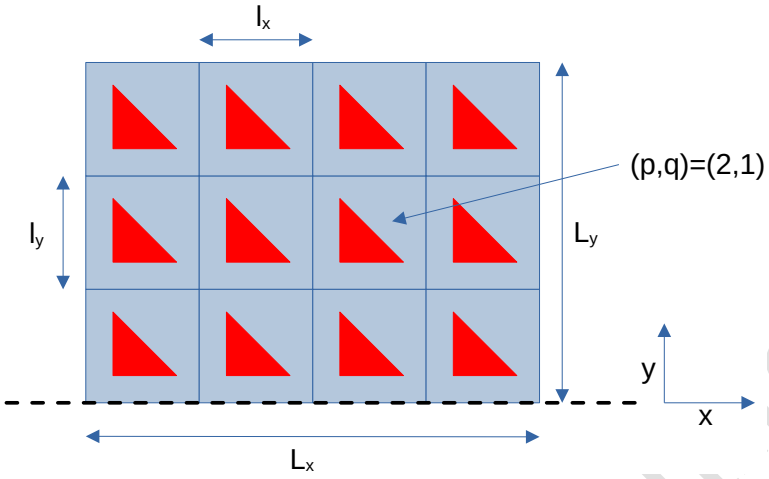

Figure 2: Non-symmetrical structure.

with

$$\begin{aligned}\mathbf{f}_L^s(q) = \frac{1}{2}(\mathbf{f}_L^{ext}(q) + \tilde{\mathbf{f}}_L^{ext}(q)) \quad &= \sum_{n=-N_y,n\ even}^{n=N_y-1} e^{i\pi qn/N_y}\left(\mathbf{F}_{Ln}^{x+}\mathbf{a}_n^{x+} - \mathbf{F}_{Rn}^{x-}(\mathbf{\Lambda}_n^{x-})^{-N_x}\mathbf{a}_n^{x-}\right)\\ &+ \frac{1}{2}\sum_{m=-N_x}^{m=N_x-1}\left(\mathbf{F}_{Lm}^{y+}(\mathbf{\Lambda}_m^{y+})^{q}\mathbf{a}_m^{y+} + \mathbf{F}_{Lm}^{y-}(\mathbf{\Lambda}_m^{y-})^{q-(N_y-1)}\mathbf{a}_m^{y-}\right)\\ &+ \frac{1}{2}\sum_{m=-N_x}^{m=N_x-1}\left(\tilde{\mathbf{F}}_{Lm}^{y+}(\mathbf{\Lambda}_m^{y+})^{N_y-1-q}\mathbf{a}_m^{y+} + \tilde{\mathbf{F}}_{Lm}^{y-}(\mathbf{\Lambda}_m^{y-})^{-q}\mathbf{a}_m^{y-}\right)\end{aligned} \tag{23}$$

and

$$\begin{aligned}\mathbf{f}_L^a(q) = \frac{1}{2}(\mathbf{f}_L^{ext}(q) - \tilde{\mathbf{f}}_L^{ext}(q)) \quad &= \sum_{n=-N_y,n\ odd}^{n=N_y-1} e^{i\pi qn/N_y}\left(\mathbf{F}_{Ln}^{x+}\mathbf{a}_n^{x+} - \mathbf{F}_{Rn}^{x-}(\mathbf{\Lambda}_n^{x-})^{-N_x}\mathbf{a}_n^{x-}\right)\\ &+ \frac{1}{2}\sum_{m=-N_x}^{m=N_x-1}\left(\mathbf{F}_{Lm}^{y+}(\mathbf{\Lambda}_m^{y+})^{q}\mathbf{a}_m^{y+} + \mathbf{F}_{Lm}^{y-}(\mathbf{\Lambda}_m^{y-})^{q-(N_y-1)}\mathbf{a}_m^{y-}\right)\\ &- \frac{1}{2}\sum_{m=-N_x}^{m=N_x-1}\left(\tilde{\mathbf{F}}_{Lm}^{y+}(\mathbf{\Lambda}_m^{y+})^{N_y-1-q}\mathbf{a}_m^{y+} + \tilde{\mathbf{F}}_{Lm}^{y-}(\mathbf{\Lambda}_m^{y-})^{-q}\mathbf{a}_m^{y-}\right)\end{aligned} \tag{24}$$

The tilde vector is obtained by reversing the order of the coefficients, for example $\tilde{f}(y) = f(L_y - y)$ on the whole structure and $\tilde{g}(y) = g(l_y - y)$ on a substructure. Note that $\mathbf{f}_L^s$ is built so that it has the same value at $y = 0$ and $y = L_y$ while $\mathbf{f}_L^a$ has opposite values at these points. With this decomposition, one can expect the convergence of the sum on n at the end points of the left and right boundaries. The same type of decomposition is made on the three other parts of the global boundary.

3.3 System to solve

The precedent relations can be written in a more compact form. For the force on the left side, one has

$$\begin{aligned}\mathbf{F}_L^s &= \boldsymbol{\omega}_y^s \mathbf{F}_L^{sx+}\mathbf{a}^{x+} - \boldsymbol{\omega}_y^s \mathbf{F}_R^{sx-}(\boldsymbol{\Lambda}^{sx-})^{-N_x}\mathbf{a}^{x-} + \mathbf{V}_L^{sy+}\mathbf{a}^{y+} + \mathbf{V}_L^{sy-}\mathbf{a}^{y-} \\ \mathbf{F}_L^a &= \boldsymbol{\omega}_y^a \mathbf{F}_L^{ax+}\mathbf{a}^{x+} - \boldsymbol{\omega}_y^a \mathbf{F}_R^{ax-}(\boldsymbol{\Lambda}^{ax-})^{-N_x}\mathbf{a}^{x-} + \mathbf{V}_L^{ay+}\mathbf{a}^{y+} + \mathbf{V}_L^{ay-}\mathbf{a}^{y-}\end{aligned} \tag{25}$$

with

$$\begin{aligned}\mathbf{F}_L^s &= \begin{pmatrix}\mathbf{f}_L^s(0)\\ \mathbf{f}_L^s(1)\\ \vdots \\ \mathbf{f}_L^s(N_y-1)\end{pmatrix}, \quad \mathbf{F}_L^a = \begin{pmatrix}\mathbf{f}_L^a(0)\\ \mathbf{f}_L^a(1)\\ \vdots \\ \mathbf{f}_L^a(N_y-1)\end{pmatrix} \\ \mathbf{F}_L^{sx+} &= diag\left(\mathbf{F}_{Ln}^{x+}\right)_{-N_y\le n\le N_y-1,\ n\ even} \\ \mathbf{F}_L^{ax+} &= diag\left(\mathbf{F}_{Ln}^{x+}\right)_{-N_y\le n\le N_y-1,\ n\ odd} \\ \mathbf{F}_R^{sx-} &= diag\left(\mathbf{F}_{Rn}^{x-}\right)_{-N_y\le n\le N_y-1,\ n\ even} \\ \mathbf{F}_R^{ax-} &= diag\left(\mathbf{F}_{Rn}^{x-}\right)_{-N_y\le n\le N_y-1,\ n\ odd} \\ \boldsymbol{\Lambda}^{sx-} &= diag\left(\boldsymbol{\Lambda}_n^{x-}\right)_{-N_y\le n\le N_y-1,\ n\ even} \\ \boldsymbol{\Lambda}^{ax-} &= diag\left(\boldsymbol{\Lambda}_n^{x-}\right)_{-N_y\le n\le N_y-1,\ n\ odd} \\ \boldsymbol{\omega}_y^s &= \left(e^{iqn\pi/N_y}\mathbf{I}_{qn}\right)_{0\le q\le N_y-1,-N_y\le n\le N_y-1,\ n\ even} \\ &= \left(\lambda_y^{qn}\mathbf{I}_{qn}\right)_{0\le q\le N_y-1,-N_y\le n\le N_y-1,\ n\ even} \\ \boldsymbol{\omega}_y^a &= \left(e^{iqn\pi/N_y}\mathbf{I}_{qn}\right)_{0\le q\le N_y-1,-N_y\le n\le N_y-1,\ n\ odd} \\ &= \left(\lambda_y^{qn}\mathbf{I}_{qn}\right)_{0\le q\le N_y-1,-N_y\le n\le N_y-1,\ n\ odd} \\ \boldsymbol{V}_L^{sy+} &= \left(\tfrac{1}{2}\left(\mathbf{F}_{Lm}^{y+}(\boldsymbol{\Lambda}_m^{y+})^q + \tilde{\mathbf{F}}_{Lm}^{y+}(\boldsymbol{\Lambda}_m^{y+})^{N_y-1-q}\right)\right)_{0\le q\le N_y-1,-N_x\le m\le N_x-1} \\ \boldsymbol{V}_L^{ay+} &= \left(\tfrac{1}{2}\left(\mathbf{F}_{Lm}^{y+}(\boldsymbol{\Lambda}_m^{y+})^q - \tilde{\mathbf{F}}_{Lm}^{y+}(\boldsymbol{\Lambda}_m^{y+})^{N_y-1-q}\right)\right)_{0\le q\le N_y-1,-N_x\le m\le N_x-1} \\ \boldsymbol{V}_L^{sy-} &= \left(\tfrac{1}{2}\left(\mathbf{F}_{Lm}^{y-}(\boldsymbol{\Lambda}_m^{y-})^{q-N_y+1} + \tilde{\mathbf{F}}_{Lm}^{y-}(\boldsymbol{\Lambda}_m^{y-})^{-q}\right)\right)_{0\le q\le N_y-1,-N_x\le m\le N_x-1} \\ \boldsymbol{V}_L^{ay-} &= \left(\tfrac{1}{2}\left(\mathbf{F}_{Lm}^{y-}(\boldsymbol{\Lambda}_m^{y-})^{q-N_y+1} - \tilde{\mathbf{F}}_{Lm}^{y-}(\boldsymbol{\Lambda}_m^{y-})^{-q}\right)\right)_{0\le q\le N_y-1,-N_x\le m\le N_x-1}\end{aligned} \tag{26}$$

with $\lambda_y = e^{i\pi/N_y}$ and $\mathbf{I}_{qn} = \mathbf{I}_{m_l\times m_l}$ with $m_l = n_{LB} + n_L$ where n_{LB} is the number of dofs in the corner LB and n_L the number of dofs in the part L of the boundary. Similar relations can be written for the three other parts of the global boundary. In matrix form, this yields the following global system

$$\begin{pmatrix}\mathbf{F}_B^s\\ \mathbf{F}_B^a\\ \mathbf{F}_R^s\\ \mathbf{F}_R^a\\ \mathbf{F}_T^s\\ \mathbf{F}_T^a\\ \mathbf{F}_L^s\\ \mathbf{F}_L^a\end{pmatrix} = \begin{pmatrix} \mathbf{V}_B^{sx+} & \mathbf{V}_B^{sx-} & \boldsymbol{\omega}_x^s\mathbf{F}_B^{sy+} & -\boldsymbol{\omega}_x^s\mathbf{F}_T^{sy-}(\boldsymbol{\Lambda}^{sy-})^{-N_y} \\ \mathbf{V}_B^{ax+} & \mathbf{V}_B^{ax-} & \boldsymbol{\omega}_x^a\mathbf{F}_B^{ay+} & -\boldsymbol{\omega}_x^a\mathbf{F}_T^{ay-}(\boldsymbol{\Lambda}^{ay-})^{-N_y} \\ -\boldsymbol{\omega}_y^s\mathbf{F}_L^{sx+}(\boldsymbol{\Lambda}^{sx+})^{N_x} & \boldsymbol{\omega}_y^s\mathbf{F}_R^{sx-} & -\mathbf{V}_R^{sy+} & -\mathbf{V}_R^{sy-} \\ -\boldsymbol{\omega}_y^a\mathbf{F}_L^{ax+}(\boldsymbol{\Lambda}^{ax+})^{N_x} & \boldsymbol{\omega}_y^a\mathbf{F}_R^{ax-} & -\mathbf{V}_R^{ay+} & -\mathbf{V}_R^{ay-} \\ -\mathbf{V}_T^{sx+} & -\mathbf{V}_T^{sx-} & -\boldsymbol{\omega}_x^s\mathbf{F}_B^{sy+}(\boldsymbol{\Lambda}^{sy+})^{N_y} & \boldsymbol{\omega}_x^s\mathbf{F}_T^{sy-} \\ -\mathbf{V}_T^{ax+} & -\mathbf{V}_T^{ax-} & -\boldsymbol{\omega}_x^a\mathbf{F}_B^{ay+}(\boldsymbol{\Lambda}^{ay+})^{N_y} & \boldsymbol{\omega}_x^a\mathbf{F}_T^{ay-} \\ \boldsymbol{\omega}_y^s\mathbf{F}_L^{sx+} & -\boldsymbol{\omega}_y^s\mathbf{F}_R^{sx-}(\boldsymbol{\Lambda}^{sx-})^{-N_x} & \mathbf{V}_L^{sy+} & \mathbf{V}_L^{sy-} \\ \boldsymbol{\omega}_y^a\mathbf{F}_L^{ax+} & -\boldsymbol{\omega}_y^a\mathbf{F}_R^{ax-}(\boldsymbol{\Lambda}^{ax-})^{-N_x} & \mathbf{V}_L^{ay+} & \mathbf{V}_L^{ay-} \end{pmatrix} \begin{pmatrix}\mathbf{a}^{x+}\\ \mathbf{a}^{x-}\\ \mathbf{a}^{y+}\\ \mathbf{a}^{y-}\end{pmatrix} \tag{27}$$

Its solution will give the amplitudes of the waves and then the forces and displacements in all substructures.

3.4 System solution

The system (27) can be written in a more compact form as

$$\mathbf{F} = \mathbf{D}_{tot}\mathbf{a} \tag{28}$$

The solution of this system is obtained by an iterative method using the GMRES algorithm. Only the product of $\mathbf{D}_{tot}$ by a vector $\mathbf{a}$ needs to be computed and matrix $\mathbf{D}_{tot}$ needs not to be built. For computing this product, one has to do the multiplication by different matrices. First the multiplication by matrices such as $\mathbf{F}_B^{sy+}$ is quite easy because such matrices are block diagonal. Matrices such as $\mathbf{\Lambda}^{sy-}$ are also diagonal. The multiplication by $\boldsymbol{\omega}_x^s$ is in fact a FFT and so neither the matrix $\boldsymbol{\omega}_x^s$ nor the multiplication by this matrix need to be done but only the FFT of a vector is used. The most difficult part is the multiplication by matrices like $\mathbf{V}_L^{sy+}$. However, such matrices involve terms like $(\lambda_{mj}^{y+})^q$. Only a limited number of propagation constants λ_{mj}^{y+} have modulus close to one and as q increases a lot of these terms are of very small amplitudes and can be neglected so that the multiplication by matrices $\mathbf{V}_L^{sy+}$ can in fact be done efficiently. So the multiplication of $\mathbf{a}$ by matrix $\mathbf{D}_{tot}$ is not so difficult and the solution of the linear system by an iterative method can be considered. For the GMRES algorithm to converge in a limited number of iterations, a preconditioner must be used. Here this is done by first computing the vector $\mathbf{Da}$ and using this result as a boundary condition for the force on the global structure which is then solved by the algorithm of the symmetrical structure as described in [31]. One expect that the solution obtained as if the structure were symmetrical will be close enough to the true solution so that it considerably reduce the number of iterations of the GMRES algorithm and constitutes a good preconditioner.

4 Numerical results

4.1 Type of computation

The behaviour of the structure is supposed described by the Helmholtz equation

$$\begin{aligned} \Delta p + k^2 p &= 0 \ \ in \ \ \Omega, \\ \frac{\partial p}{\partial n} &= q_0 \ \ over \ \partial\Omega \end{aligned} \tag{29}$$

with $k = \omega/c$, ω the circular frequency and $c = 343m/s$ the sound velocity in case of acoustic propagation. The structure Ω is divided into $N_x \times N_y$ substructures of size $L_x \times L_y$ (with generally $L_x = L_y = 0.1m$). q_0 is a given function on the boundary. Two types of boundary conditions are used here. The first one is created by a point source outside the structure such as $p_0(\mathbf{x}) = \frac{i}{4}H_0(k|\mathbf{x}-\mathbf{x}_s|)$ for a point source $\mathbf{x}_s$ outside the domain Ω and $q_0 = \frac{\partial}{\partial n}p_0$ while the second one is obtained by taking q_0 equals to one on a part of the boundary. We generally compare the results of a full Finite Element Method (FEM) solution and the present two-dimensional WFE method for different structures.

4.2 Triangle structures

We first start by computing the three types of triangle structures presented in Figure 3. The first two substructures have respectively a symmetry plane along y and x while the last one is completely non-symmetrical along the coordinate axes.

As a first example, a structure made of 5×5 substructures is computed at $2000Hz$. The boundary condition is obtained by a point source at $(-0.5m, -0.5m)$. Figure 4 compares the results of a classical FEM computation, the present two-dimensional WFE and the computation with the method described in [31] where the substructures are supposed symmetrical. A very good agreement is observed between the present method and the FEM computation while the results of the computation assuming a symmetrical structure is quite different and false.

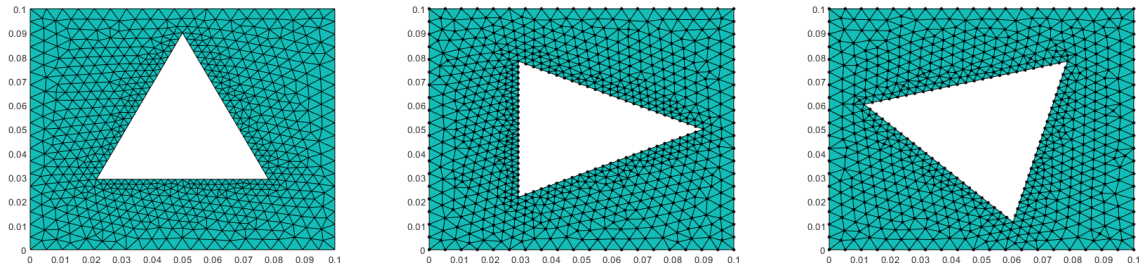

Figure 3: Triangle substructures with vertical symmetry (left), horizontal symmetry (middle) and without symmetry (right).

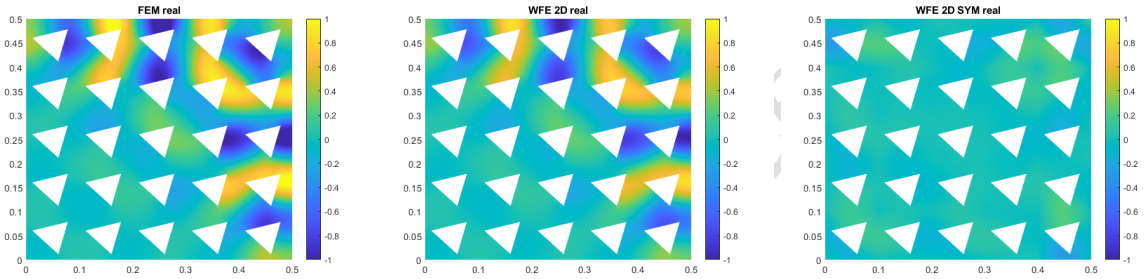

Figure 4: FEM computation (left), present method (middle) and method assuming a symmetrical structure (right).

In Figure 5, the number of iterations for the convergence of the GMRES algorithm is plotted versus the frequency for structures with 5×5 and 50×50 substructures. One can observe that completely non-symmetrical substructures lead to a larger number of iterations while substructures that has a plane symmetry are much easier to solve. The number of iteration increases with the frequency for completely non-symmetrical structures while the frequency seems to have very little influence in the other cases. One can also see that the influence of the number of substructures is small because the number of iterations is not very different for 5×5 and 50×50 substructures.

4.3 Structures with cavities

We consider in this case the two substructures shown in Figure 6. These are cavities, one being symmetrical relative to an axis parallel to x while the other is fully non-symmetrical. We study here the transmission factor defined by

$$T_{left\ to\ right} = \frac{\left(\sum_{node\ i\ on\ right\ boundary} |u_i|^2\right)^{1/2}}{\left(\sum_{node\ i\ on\ left\ boundary} |u_i|^2\right)^{1/2}} \tag{30}$$

thus the square average of the solution on the right boundary over the solution on the left boundary. The term u_i is the solution at node i for a uniform pressure applied at the left boundary ($q_0 = 1$ on the left boundary and 0 elsewhere). We consider the case of a global structure made of 5×5 substructures. One can also define $T_{right\ to\ left}$ in a similar way. In case of symmetrical structure, one should have $T_{left\ to\ right} = T_{right\ to\ left}$. In Figure 7, the transmission factors are plotted for three substructures. On the left, the case of the symmetrical cavity on the left of Figure 6 is plotted while the curves in the middle is for the fully non-symmetrical cavity. Both curves show a different behavior according to the propagation direction. Note that this is especially the case in the band gaps. Finally, the right curves in Figure 7 show the case with a circular cavity of radius $0.02m$ in the center of the substructure. As this structure is fully symmetric, the

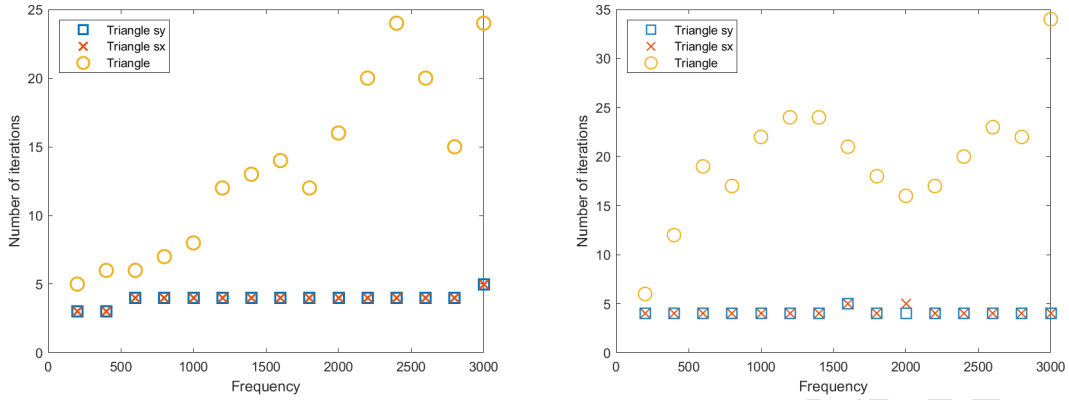

Figure 5: Number of iterations for 5×5 substructures (left) and 50×50 substructures (right).

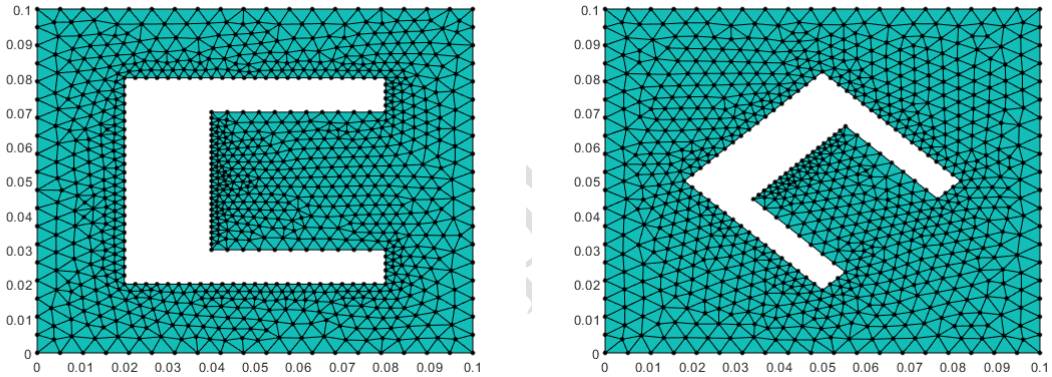

Figure 6: Cavity with symmetry (left) and without symmetry (right).

propagation is exactly the same in the two directions.

In Figure 8 the computing time for the FEM and the present WFE method are plotted for structures of increasing sizes $N \times N$ with a substructure made of the fully non symmetrical cavity of the right of Figure 6 at $500Hz$ for the boundary condition obtained from the outside point source as before. This case is the most difficult to solve by the present method. The results show the efficiency of the present method. In the case of a structure with 250×250 substructures, the present method is 32 times faster than the FEM. For a larger number of substructures the FEM computation runs out of memory on the PC Intel(R) Core(TM) i9-12900 with 64Go of memory used for these computations. The two-dimensional WFE has not these limitations. In the case of the WFE two results are plotted. First the time needed to compute the amplitudes of the waves (or solving systems (27), (28)) is plotted (curve WFE 2D comp in the figure). The remaining time is used by the post-processing to get the solution at each node from the wave amplitudes and the global time is the curve denoted WFE 2D tot in the figure. For structures larger than 350×350 it can take some time and consume memory so that the post-processing has not been done. In such a case, it would be better to get the solution only on a limited part of the structure or to take some form of averaging on each substructure. On the right of Figure 8, the number of iterations for the GMRES is plotted versus the frequency for cavities with or without symmetries and for standard or fine meshes. The fine mesh is obtained by doubling the number of nodes of figure 6 along each side. It can be seen that the density of the mesh has a low influence on the number of iterations while the symmetry of the structure seems very important.

In figure 9 the case of a large structure made of 200×200 substructures with non-symmetrical cavities is plotted for the frequencies 1500 Hz. The left picture is for a uniform load on the left boundary (and all other three parts of the boundary are free) while the right picture is for a uniform load on the right boundary. One

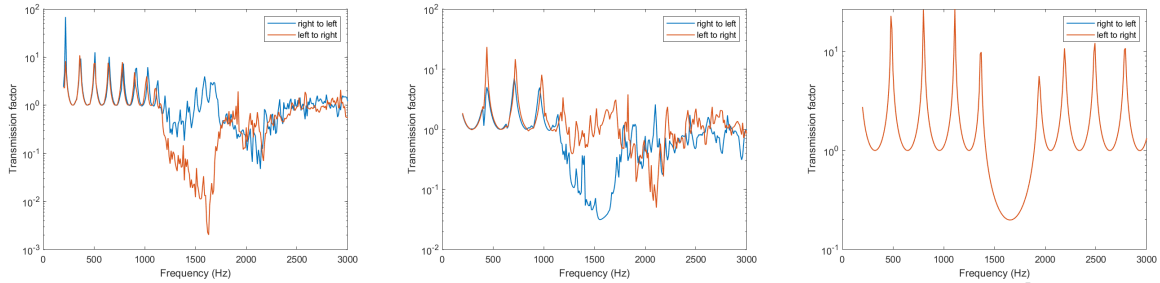

Figure 7: Transmission factor for symmetrical cavity (left), non-symmetrical cavity (middle) and circular cavity (right).

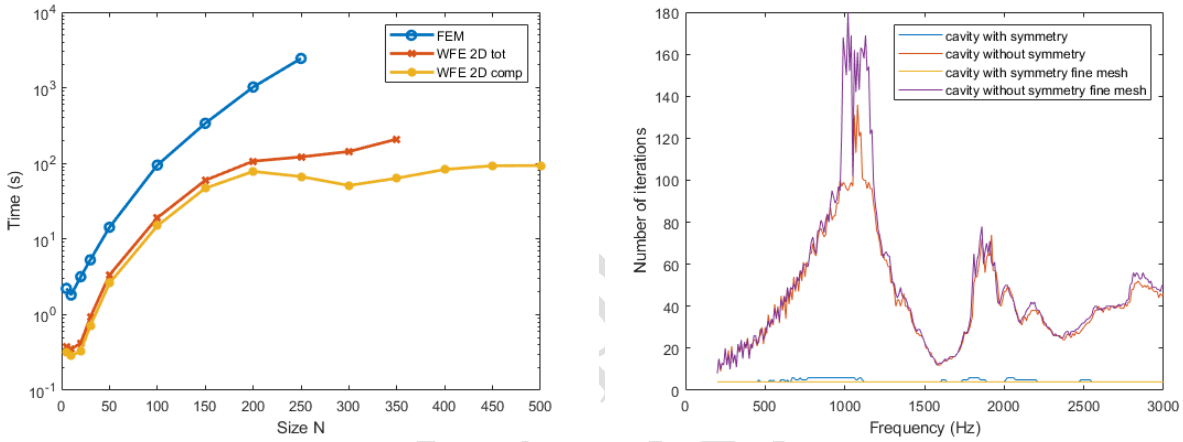

Figure 8: Computing times for the FEM and the WFE methods (left) and number of iterations for the WFE (right).

can see that there is little propagation from the left to the right while the propagation in the other direction much easier.

In figure 10, the error between the FEM and WFE solutions and the amplitudes of the solution are plotted versus the frequency for four cases: standard mesh for cavities with and without symmetries and fine mesh for the same two structures. The structure is made of 50×50 substructures. This error is defined as:

$$e = \frac{\left(\sum_{i \text{ on whole mesh}} |u_i^{fem} - u_i^{wfe}|^2\right)^{1/2}}{\left(\sum_{i \text{ on whole mesh}} |u_i^{fem}|^2\right)^{1/2}} \tag{31}$$

It can be seen that the error is very small for symmetrical cavities and larger for non-symmetrical cavities. However the error is reduced with a fine mesh and it seems localized around specific frequencies probably associated to resonances of the structure.

5 Conclusion

We have extended the computation of two-dimensional periodic media to the case of non-symmetrical structures. The accuracy of the result is equivalent to a full FEM computation but with a much lower computing time for large structures. Although an iterative method such as the GMRES is used for the solution, the number of iterations does not seem very sensible to the number of substructures but rather to the degree of

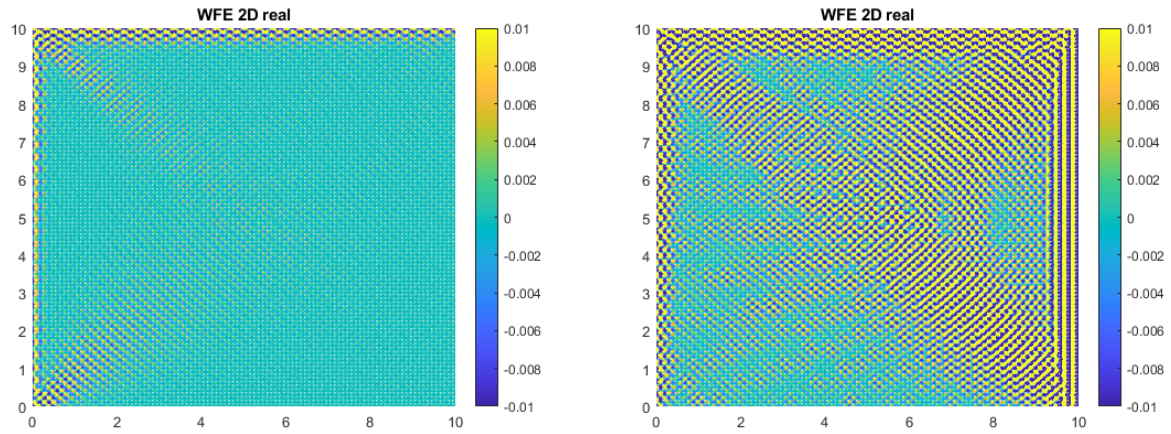

Figure 9: Solutions for a 200×200 non-symmetrical cavity structure at 1500 Hz with uniform load on the left boundary (left) and on the right boundary (right).

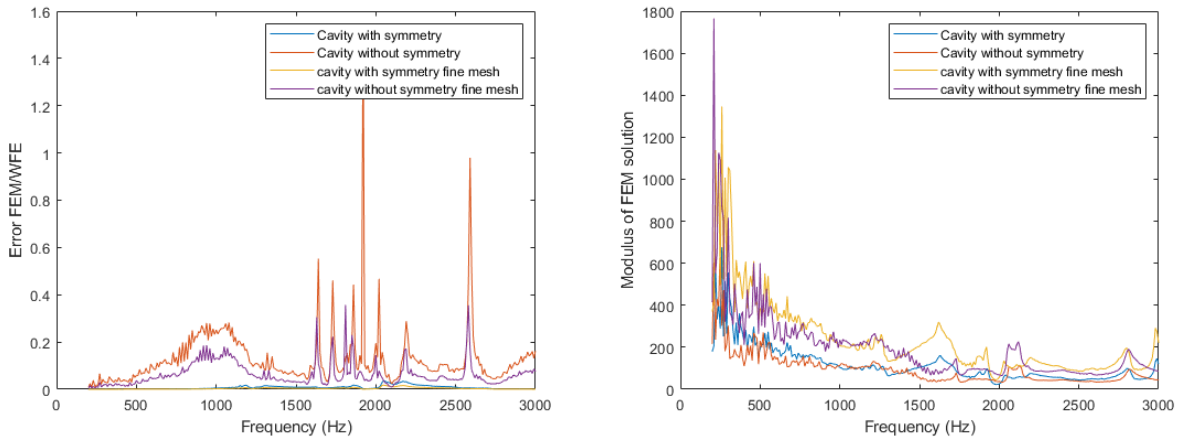

Figure 10: Relative errors between the FEM and WFE solutions (left) and amplitudes of FEM solution (right).

symmetry of the substructure. Examples show the influence of the lack of symmetry of the structures for example by allowing the propagation in a direction, but not in the reverse direction. We are limited here to scalar equations and future researches should try to extend it to vector equations such as for two-dimensional elasticity.

References

[1] B. Mace, D. Duhamel, M. Brennan, and L. Hinke, "Finite element prediction of wave motion in structural waveguides," *Journal of the Acoustical Society of America*, vol. 117, pp. 2835–2843, 2005.

[2] D. Duhamel, B. R. Mace, and M. J. Brennan, "Finite element analysis of the vibrations of waveguides and periodic structures," *Journal of Sound and Vibration*, vol. 294, no. 1-2, pp. 205–220, 2006.

[3] J.-M. Mencik and D. Duhamel, "A wave-based model reduction technique for the description of the dynamic behavior of periodic structures involving arbitrary-shaped substructures and large-sized finite element models," *Finite Elements in Analysis and Design*, vol. 101, pp. 1–14, 2015.

[4] J.-M. Mencik and D. Duhamel, "A wave finite element-based approach for the modeling of periodic structures with local perturbations," *Finite Elements in Analysis and Design*, vol. 121, pp. 40–51, Nov. 2016.

[5] J.-M. Mencik, "New advances in the forced response computation of periodic structures using the wave finite element (WFE) method," *Computational Mechanics*, vol. 54, no. 3, pp. 789–801, 2014.

[6] T. Hoang, D. Duhamel, and G. Foret, "Wave finite element method for waveguides and periodic structures subjected to arbitrary loads," *Finite Elements in Analysis and Design*, vol. 179, p. 103437, 2020.

[7] J. M. Renno and B. R. Mace, "On the forced response of waveguides using the wave and finite element method," *Journal of Sound and Vibration*, vol. 329, no. 26, pp. 5474–5488, 2010.

[8] A. Abdel-Rahman, "Matrix analysis of wave propagation in periodic systems," Ph.D. dissertation, University of Southampton, 1979.

[9] R. S. Langley, "A note on the force boundary conditions for two-dimensional periodic structures with corner freedoms," *Journal of Sound and Vibration*, vol. 167, no. 2, pp. 377–381, 1993.

[10] A. S. Phani, J. Woodhouse, and N. A. Fleck, "Wave propagation in two-dimensional periodic lattices," *The Journal of the Acoustical Society of America*, vol. 119, no. 4, pp. 1995–2005, 2006.

[11] E. Manconi, "Modelling wave propagation in two–dimensional structures using a wave/finite element technique," Ph.D. dissertation, University of Parma, 2008.

[12] C. W. Zhou, J. P. Lainé, M. N. Ichchou, and A. M. Zine, "Multi-scale modelling for two-dimensional periodic structures using a combined mode/wave based approach," *Computers & Structures*, vol. 154, pp. 145–162, 2015.

[13] A. Palermo and A. Marzani, "Extended Bloch mode synthesis: Ultrafast method for the computation of complex band structures in phononic media," *International Journal of Solids and Structures*, vol. 100-101, pp. 29–40, 2016.

[14] D. Krattiger and M. I. Hussein, "Bloch mode synthesis: Ultrafast methodology for elastic band-structure calculations," *Phys. Rev. E*, vol. 90, p. 063306, Dec 2014.

[15] D. Krattiger and M. I. Hussein, "Generalized Bloch mode synthesis for accelerated calculation of elastic band structures," *Journal of Computational Physics*, vol. 357, pp. 183–205, 2018.

[16] M. I. Hussein, "Reduced Bloch mode expansion for periodic media band structure calculations," *Proc. R. Soc. A.*, vol. 465, p. 2825–2848, 2009.

[17] T. F. Eibert, J. L. Volakis, D. R. Wilton, and D. R. Jackson, "Hybrid FE/BI modeling of 3-D doubly periodic structures utilizing triangular prismatic elements and an MPIE formulation accelerated by the Ewald transformation," *IEEE Transactions on Antennas and Propagation*, vol. 47, no. 5, 1999.

[18] D. Duhamel, "Finite element computation of Green's functions," *Engineering Analysis with Boundary Elements*, vol. 31, no. 11, pp. 919–930, 2007.

[19] J. M. Renno and B. R. Mace, "Calculating the forced response of two-dimensional homogeneous media using the wave and finite element method," *Journal of Sound and Vibration*, vol. 330, no. 24, pp. 5913–5927, 2011.

[20] J.-F. Lu, J. Cheng, and Q.-S. Feng, "Plane wave finite element model for the 2-D phononic crystal under force loadings," *European Journal of Mechanics - A/Solids*, vol. 91, p. 104426, 2022.

[21] R. S. Langley, "The response of two-dimensional periodic structures to point harmonic forcing," *Journal of Sound and Vibration*, vol. 197, no. 4, pp. 447–469, 1996.

[22] R. S. Langley, "The response of two-dimensional periodic structures to impulsive point loading," *Journal of Sound and Vibration*, vol. 201, no. 2, pp. 235–253, 1997.

[23] I. Andonegui and A. J. Garcia-Adeva, "The finite element method applied to the study of two-dimensional photonic crystals and resonant cavities," *Optics Express*, vol. 21, no. 4, pp. 4072–4092, Feb 2013.

[24] J.-M. Mencik and M.-L. Gobert, "Acoustic radiation of 2D nearly periodic metamaterial plates via finite element procedures and model reduction strategies," in *International Conference on Noise and Vibration Engineering (ISMA 2022)*, Leuven, Belgium, 12-14 Sep., 2022, pp. 3013–3022.

[25] L. Van Belle, C. Claeys, E. Deckers, and W. Desmet, "Fast forced response calculations of finite metamaterial plates using a generalized Bloch mode synthesis based sub-structuring approach," in *Proceedings of Euronoise*, Madeira, Portugal, 25-27 October, 2021, pp. 1–10.

[26] F. Qu, L. Van Belle, and E. Deckers, "A unit cell wave based reduced order modelling approach for fast vibration response calculations of finite periodic metamaterial plates," in *International Conference on Noise and Vibration Engineering (ISMA 2022)*, Leuven, Belgium, 12-14 Sep., 2022, pp. 3133–3147.

[27] S. van Ophem, E. Deckers, and W. Desmet, "Efficient assembly of unit cells with Krylov based model order reduction," in *International Conference on Noise and Vibration Engineering (ISMA 2018)*, Leuven, Belgium, 17-19 September, 2018, pp. 445–456.

[28] M. Shadi Mohamed, M. Seaid, J. Trevelyan, and O. Laghrouche, "A partition of unity FEM for time-dependent diffusion problems using multiple enrichment functions," *International Journal for Numerical Methods in Engineering*, vol. 93, no. 3, pp. 245–265, 2013.

[29] M. S. Mohamed, O. Laghrouche, and J. Trevelyan, "A q-adaptive partition of unity finite element method for the solution of the 2-D helmholtz equation," *IOP Conference Series: Materials Science and Engineering*, vol. 10, no. 1, p. 012148, jun 2010.

[30] M. Malek, N. Izem, M. Seaid, M. S. Mohamed, and M. Wakrim, "A partition of unity finite element method for nonlinear transient diffusion problems in heterogeneous materials," *Computational and Applied Mathematics*, vol. 38, no. 2, p. 31, Mar 2019.

[31] D. Duhamel, "Computation of the dynamic scalar response of large two-dimensional periodic and symmetric structures by the wave finite element method," *Finite Elements in Analysis and Design*, vol. 230, p. 104096, 2024.